www.czasopisma.pan.pl PAN POLSKA AKADEMIA NAUK www.journals.pan.pl

Arch. Metall. Mater. **67** (2022), 3, 1107-1116

DOI: https://doi.org/10.24425/amm.2022.139710

J. PIEKŁO[1], A. GARBACZ-KLEMPKA[1*]

ANALYSIS OF FAILURE PROCESS OF MARAGING STEEL PRODUCED BY SELECTIVE LASER MELTING (SLM)

An investigation of the failure process of maraging steel grade X3NiCoTi18-9-5 produced by the SLM method that is subjected to various three-dimensional stress-states has been carried out. In this paper, deformations and damage evolution are analysed experimentally and numerically. Three microstructures of the SLM steel were obtained after the appropriate heat treatment. Tensile tests of smooth specimens and axisymmetric notched specimens have been performed. Numerical models of the samples with ring notches were made in order to determine the stress state and displacement field in the notch area at the moment of the sample's breakage as well as to compare the experimentally determined effective strain in the notch after the sample's breakage with the deformation being calculated on the basis of the numerical solution. As a result of the research, it was found that the type of fracture of samples obtained from X3NiCoTi18-9-5 steel powder by the SLM method depends on the size of the ring notch's radius. Based on the performed numerical calculations and experimental tests, it was found that, for each of the analysed variants of heat treatment, it was possible to indicate the approximate limit value of triaxiality factor T_f, above which there is a scrap of brittle X3NiCoTi18-9-5 steel produced by the SLM method. This value is determined by the characteristic bending of the function that determines the relationship between triaxiality factor T_f and effective strain e_{eff}.

Keywords: Selective Laser Melting; Maraging steel; Heat treatment; Metalography; Mechanical Properties; Computer modelling

1. Introduction

The SLM process is one of the methods for the incremental AM manufacturing of a detail by fusing processed material into a powdered form, thus filling the working chamber [1-4]. The major advantage of this method is geometrical freedom; this allows for the capability of fabricating parts of very complex shapes with a smallest feature size of about 100 μm [5]. However, some restrictions on the shape are given by the requirements of unsolidified material removal from internal cavities and the need of supports to sustain overhangs [6]. Due to the nature of the SLM process, products are prone to different types of defects (e.g. porosities, inclusions, voids, cavities, micro-cracks, shrinkage, lack of fusion, etc.); this increases the uncertainty of their mechanical behaviour [7-9]. Therefore, a good understanding of structural integrity under monotonic and cyclic loading in uniaxial and triaxial stress states is critical for expanding the range of applications and developing more-responsible parts of a structure. A material's resistance is usually estimated during a uniaxial tensile test, although the material is usually subjected to multiaxial stress states in many parts of a structure. In a multiaxial stress state, the properties of the material and its method of decohesion change with the value of the ratio of the stress-state triaxiality. In continuum mechanics, stress triaxiality is the relative degree of hydrostatic stress in a given stress state. It is commonly used as the triaxiality factor T_f, which is the ratio of the hydrostatic stress σ_m to the von Mises equivalent stress σ_{eq} [10]:

$$T_f = \frac{\sigma_m}{\sigma_{eq}} \tag{1}$$

The triaxiality factor T_f has important applications in fracture mechanics and can often be used to predict the type of fracture (i.e. ductile or brittle) within a region that is defined by this stress state [11-13]. High-stress triaxiality promotes brittle cleavage fractures as well as dimple formation within an otherwise ductile fracture. According to Bidgman's solution [14], the triaxial factor T_f in their central part is equal in samples with a ring notch ρ and sample radius R in the plane of the notch bottom:

$$T_f = \frac{1}{3} + \ln\left(1 + \frac{R}{2\rho}\right) \tag{2}$$

[1] AGH UNIVERSITY OF SCIENCE AND TECHNOLOGY, FACULTY OF FOUNDRY ENGINEERING, AL. MICKIEWICZA 30, 30-059 KRAKÓW, POLAND

* Corresponding author: agarbacz@agh.edu.pl

© 2022. The Author(s). This is an open-access article distributed under the terms of the Creative Commons Attribution-NonCommercial License (CC BY-NC 4.0, https://creativecommons.org/licenses/by-nc/4.0/deed.en which permits the use, redistribution of the material in any medium or format, transforming and building upon the material, provided that the article is properly cited, the use is noncommercial, and no modifications or adaptations are made.

Maraging steels are good candidates for the SLM process because of their good weldability, which results from their lack of interstitial alloy elements and their resistance to quench cracking due to their low carbon content. The microstructure of SLM-produced parts depends on the powder chemical composition and properties; however, it is mainly related to the values of the process parameters that are used for printing [15]. Maraging steels are ultra-high-strength Fe-Ni alloys that are mainly developed for aircraft, aerospace, and tooling applications. Using the SLM process, it is possible to make certain parts of pressure moulds that are intended for casting Al-Si alloys from the powders of the maraging steel grade X3NiCoTi18-9-5 [16-18]. With a good combination of strength and toughness, steel grade X3NiCoTi18-9-5 results from the ageing of a relatively soft martensite that is formed by cooling from an Ni-containing γ-Fe solid solution. This ageing leads to the formation of strengthening precipitates [19-21]. Fine $Ni_3(Al, Ti, Mo)$ and Fe_2Mo intermetallic particles are precipitated during ageing treatments from 500° to 550°C, which result in the high hardness and strength of these alloys [22]. The alloy produced by SLM repeatedly undergoes reheating. This repetitive heating can act as an intrinsic heat treatment during the process, which facilitates the nucleation of the intermetallic precipitates without a post-heat treatment [23]. Therefore, the precipitation can occur easily without solution heat treatments. As a result, the supersaturation process is omitted and is reduced to ageing for the maraging steel produced by SLM [24].

2. Materials and methods

Maraging steel in the form of CL50WS gas-atomised powder was used as the raw material. The chemical composition of the powder corresponds to steel marked with the DIN X3NiCoMoTi18-9-5 symbol, which is a high-strength, martensitic, and age-hardenable hot-work steel. The chemical composition of the powder (determined on the basis of spectroscopic tests) is listed in TABLE 1.

TABLE 1

Chemical composition wt.% of studied powder

Chemical Composition wt.%				
Ni	**Mo**	**Co**	**Ti**	**Fe**
18.1	5.2	9.6	1.1	65.2

Fig. 1 shows the SEM morphology of the powder, and Fig. 2 shows its size distribution as measured by a Fritsch Analysette 22 NanoTech laser-scattering particle-size analyser.

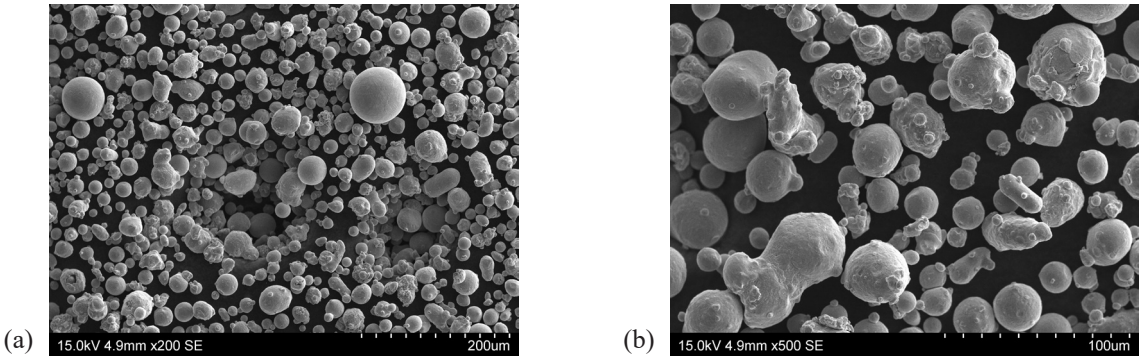

Fig. 1. Scanning electron microscopy (SEM) morphology of X3NiCoMoTi18-9-5-grade maraging steel powder: (a) Image of steel powder; (b) different grain sizes marked

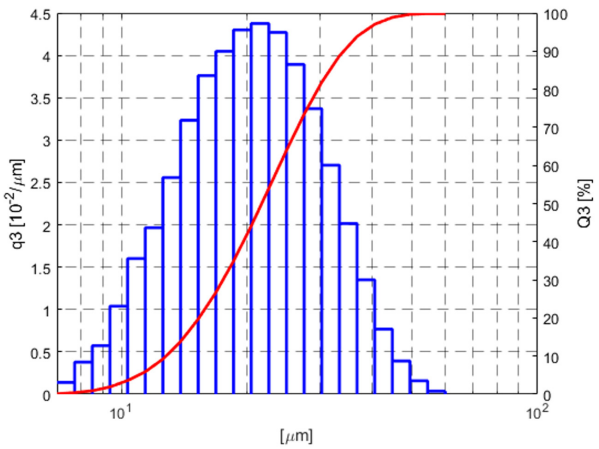

Fig. 2. Size distribution of X3NiCoMoTi18-9-5-grade maraging steel powder [17]

Powder that was previously used to print SLM parts was used in our research. The powder particles had a median particle size of cumulative volume distribution $x_{50.3}$ = 23.56 μm. The minimum and maximum particle sizes were x_{min} = 7 μm and x_{max} = 62 μm, respectively, and the particles were spherical or quasi-spherical in shape (Fig. 1). This shape allowed the particles to flow without hindrance during deposition. The samples for the testing and the sprue spreader were made using the M2 Concept Laser Cusing device. The material was printed in a nitrogen atmosphere with the parameters listed in TABLE 2.

The island-scanning pattern was used in order to minimise the effect of thermal-induced stresses in the components. In this scanning strategy, part of the surface of each slice was divided into small square islands of 5 × 5 mm. The islands were scanned in a random manner, while the scanning direction was altered

TABLE 2

Selective laser melting (SLM) process parameters

SLM Parameter	
Laser power (W)	180
Laser speed (mm/s)	1100
Laser beam diameter (μm)	80
Layer thickness (μm)	25
Hatch space (μm)	90

at a right angle with respect to the neighbouring islands. The relative density (ρ_r) of the fabricated specimens was measured by formula $\rho_r = (m_0\rho_1)/(m_0\rho_0 - m_1\rho_0)$ according to Archimedes' principle, in which m_0, ρ_0, m_1, and ρ_1 are the maraging steel specimen's weight in air, its theoretical full-density (8.05 g/cm^3), its weight when submerged in water, and the density of the applied water under normal atmospheric pressure, respectively. The relative density of the fabricated specimens reached 99.91%.

The samples were made directly using the SLM printing method and subjected to three heat treatments: "490" – ageing at 490°C for 6 hours; "540" – ageing at 540°C for 6 hours; and "585" – ageing at 585°C for 6 hours. The heating and cooling took place at a speed of 100°C/h. The axis of each printing sample was perpendicular to the plane of the base plate of the SLM device.

Uniaxial tensile tests were carried out on specimens with a diameter of 5 mm using an MTS 810 testing machine. An MTS extensometer with a 20-mm base was used to measure the elongation. The specimens that were intendend to be subjected to investigations in a multiaxial stress-state had circumferential notches with different radii of ρ = 0.5, 1.5, 2.5, 3.5, 4.5, and 6.5 mm (as shown in Fig. 3). The diameter all specimens was D = 10 mm, and the minimal diameter at the notch was d = 5 mm.

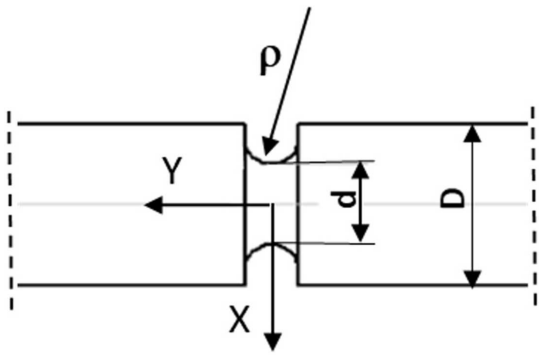

Fig. 3. Notched specimen for tensile tests in triaxial stress-state

During the tensile tests, the load changes were recorded. The tensile test was performed until each specimen failed. The diameter notch changes (Dd) were measered before and after the tensile tests using an optical microscope and instrumentation for fixing the sample.

The metallographic tests of the microsections and fractures were performed using a Nikon SMZ 745T stereoscopic optical microscope, a Nikon Eclipse metallographic microscope with a DsFi1 camera that enabled digital-image analysis, and a HITACHI S-3400N scanning electron microscope with Thermo Noran energy dispersive X-ray spectroscopy. Chemical composition tests were also carried out using energy dispersive X-ray fluorescence (ED-XRF) via a SPECTRO MIDEX spectrometer. The numerical calculations that were used to determine the stress field in the notch zones were performed with a Dassault System Simulia Abaqus v.2019 [25].

3. Experimental results

Mechanical testing

The resistance properties of the maraging steel that was made directly using the SLM printing method were determined during the course of the uniaxial tensile tests. As a result of these tests, the ultimate tensile stress UTS, yield stress $\sigma_{p0.2}$, modulus of elasticity E, total elongation A, and logarithmic strains e were obtained. The results of the tensile tests on the uniaxial stress-state of the specimens that were subjected to three variants of heat treatment and without heat treatment are listed in TABLE 3.

To analyse the fracture surface morphology, the samples were examined under different stress states. During the tensile tests of the samples with ring notches, the maximum force and effective strain ε_{eff} were determined by Formula [26]:

$$\varepsilon_{eff} = 2\ln\left(\frac{d_o}{d}\right) \tag{3}$$

where:

d_o – initial specimen diameter at minimal notched cross-section;

d – final specimen diameter at minimal notch cross-section.

Fig. 4 shows the relationship between the triaxiality factor T_f and the load at the moment of the SLM-steel's failure without heat treatment and after heat treatment variants "490", "540", and "585".

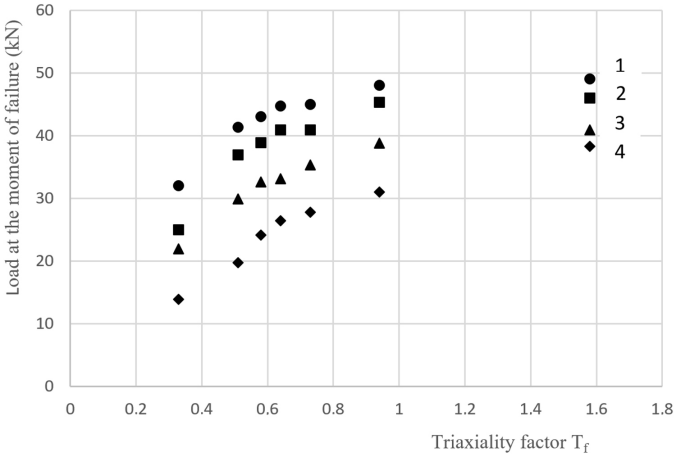

Fig. 4. Diagram of values describing load at moment of failure as function of triaxiality factor T_f: 1 – heat treatment "490"; 2 – heat treatment "540"; 3 – heat treatment "585"; 4 – alloy not heat-treated

The curves in Fig. 5 show the strong relationship between the effective strain ε_{eff} at the moments of the failures of the SLM steel specimens and the triaxiality factor T_f as well as the heat-treatment temperature.

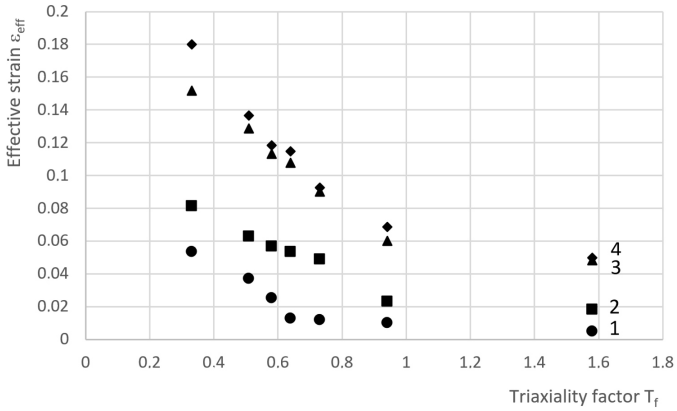

Fig. 5. Diagram of values describing effective strain e_{eff} at moment of failure as function of triaxiality factor T_f: 1 – heat treatment "490"; 2 – heat treatment "540"; 3 – heat treatment "585"; 4 – alloy not heat-treated

Microstructural characterization

The microstructure of the built samples is different from a typical martensite microstructure, which contains primary austenite grains as well as martensite packages, blocks, and tiles (Fig. 6a). Heat treatment at 490°C does not cause grain growth and nor changes the original shapes of the cells (Fig. 6b). Ageing at 540°C causes grain growth as well as changes in the shapes of the cells. The share of the secondary austenite, which separates at the grain boundary, also increases (Fig. 6c). As a result of ageing at 585°C, the original shapes of the cells disappear due to the release of the austenite phase – not only at the grain boundaries, but also inside the cells (Fig. 6d).

Fractography

The main aim of the fractographic examination was to make an qualitative assessment of the fracture morphology in relation to the stress triaxiality factor. Examinations were made on all of the specimens that were tested under different spatial stress states. Several photos were taken at different magnifications of the microregion in the center of each sample. These examinations indicated that the stress state influenced the fracture surface morphology. Fig. 7 shows the typical fracture images of the test specimens with an untreated SLM steel alloy, which were typical for six different values of triaxiality factor T_f.

The fractures of the ring-notched samples with triaxiality factors (T_f) of 0.94 and 1.58 are visible in Figs. 7e and 7f. In the case of the other lower values of T_f, plastic fracturing dominates (Figs. 7a-d). Fig. 8 collects and compares the images of the fractures of the ring samples for two variants of ageing: 585°C (first column), and 490°C (second column).

As for the untreated steel, the fractures of the samples that were aged at 585°C show the features of brittle fracturing for T_f = 0.94 and T_f = 1.58 (Figs. 8g and 8i). In the remaining photos that are shown in the first column, plastic fracturing

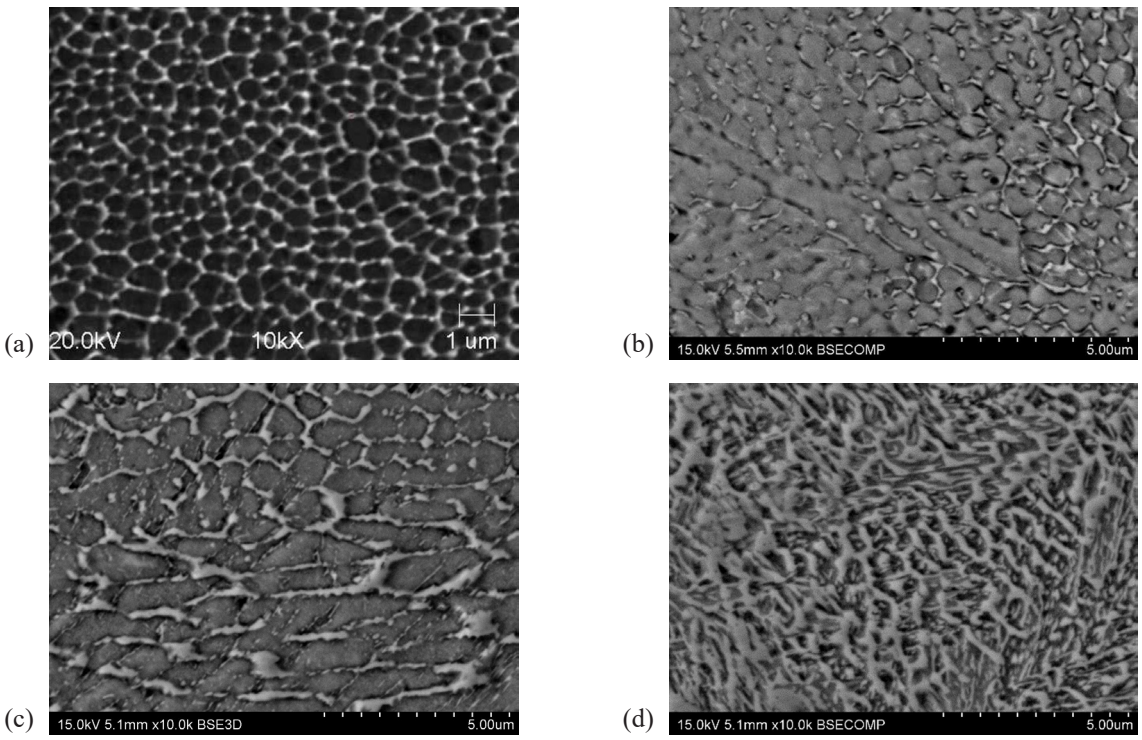

Fig. 6. Images of alloy microstructure: (a) after solidification; (b) heat treatment "490"; (c) heat treatment "540"; (d) heat treatment "585" (taken with scanning microscope; etched 4% picral solution)

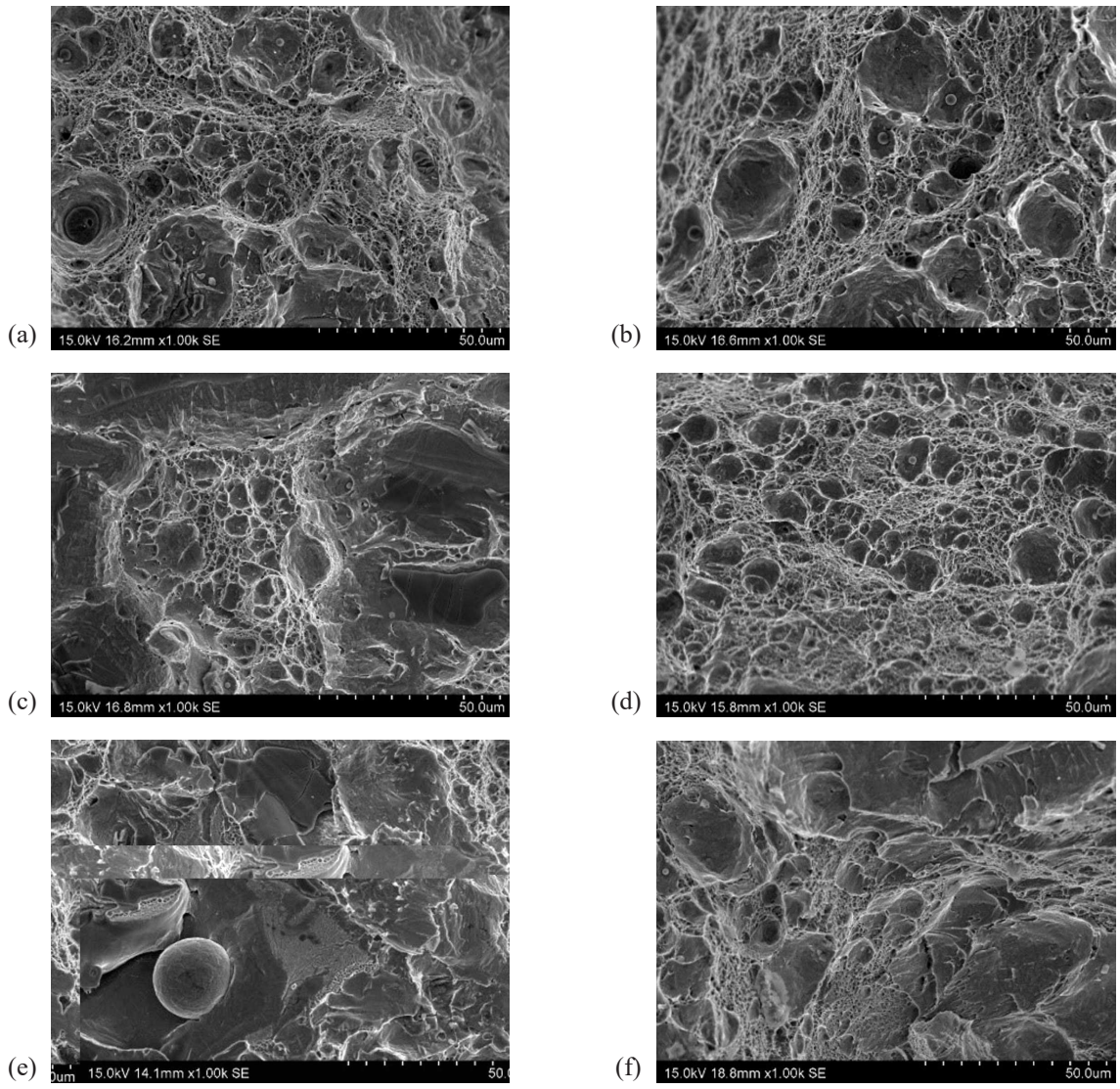

Fig. 7. Specimen fracture for different levels of triaxiality factor T_f: (a) 0.51; (b) 0.58; (c) 0.64; (d) 0.73; (e) 0.94; (f) 1.58 (alloy not heat-treated)

dominates (Figs. 8a,c,e). Ageing at 490°C increases the strength of the SLM steel at the expense of its plastic properties. In the observed sample, brittle fracturing dominates almost the entire tested range of the triaxiality factor T_f (Figs. 8d,f,h,j). Only for triaxiality factors T_f = 0.51 and T_f = 0.64 are small areas of plastic fracture visible in the samples.

Numerical model

Numerical models of the samples with ring notches were made in order to determine the stress state and the displacement field in the notch areas at the moment of each sample's breakage as well as to compare the experimentally determined effective strain in each notch after each sample's breakage with the deformation of each calculated on the basis of its numerical solution. The model uses nonlinear axisymmetric elements. The material properties were adopted on the basis of the averaged values that were obtained in the static tensile tests that were carried out on the smooth samples after the "490", "540", "585", and not heat-treated variants. The description of the tensile test diagram's true stress in terms of the elastic and plastic true strains was determined in tabular form.

Figs. 9 and 10 each show a typical image of the stress field before fracture (which are representative of the different radii of the ring notches) of the specimens made of SLM steel and heat-treated according to variants "490", "540", and "585". The stress field that was determined by the FEM method (shown in Fig. 9) is typical for a fracture that is characterised by a high proportion of plastic deformation zones. At the moment that preceded the decohesion of the material, the maximum stress σ_y is in the axis of the specimen in the place that is indicated in Fig. 9b. In turn, the highest value of the equivalent stress σ_{eq} occurs over the entire notch cross-section in the area that is indicated in Fig. 9a.

The stress field shown in Fig. 9 is consistent with Bridgman's theoretical solution Eq. (2) for the ductile fracture case. The results of the calculations that are shown in Fig. 9 can be obtained only when the non-linear relationship between the stress and strain is taken into account in the numerical model. If the fracture's surface is dominated by a share of those areas

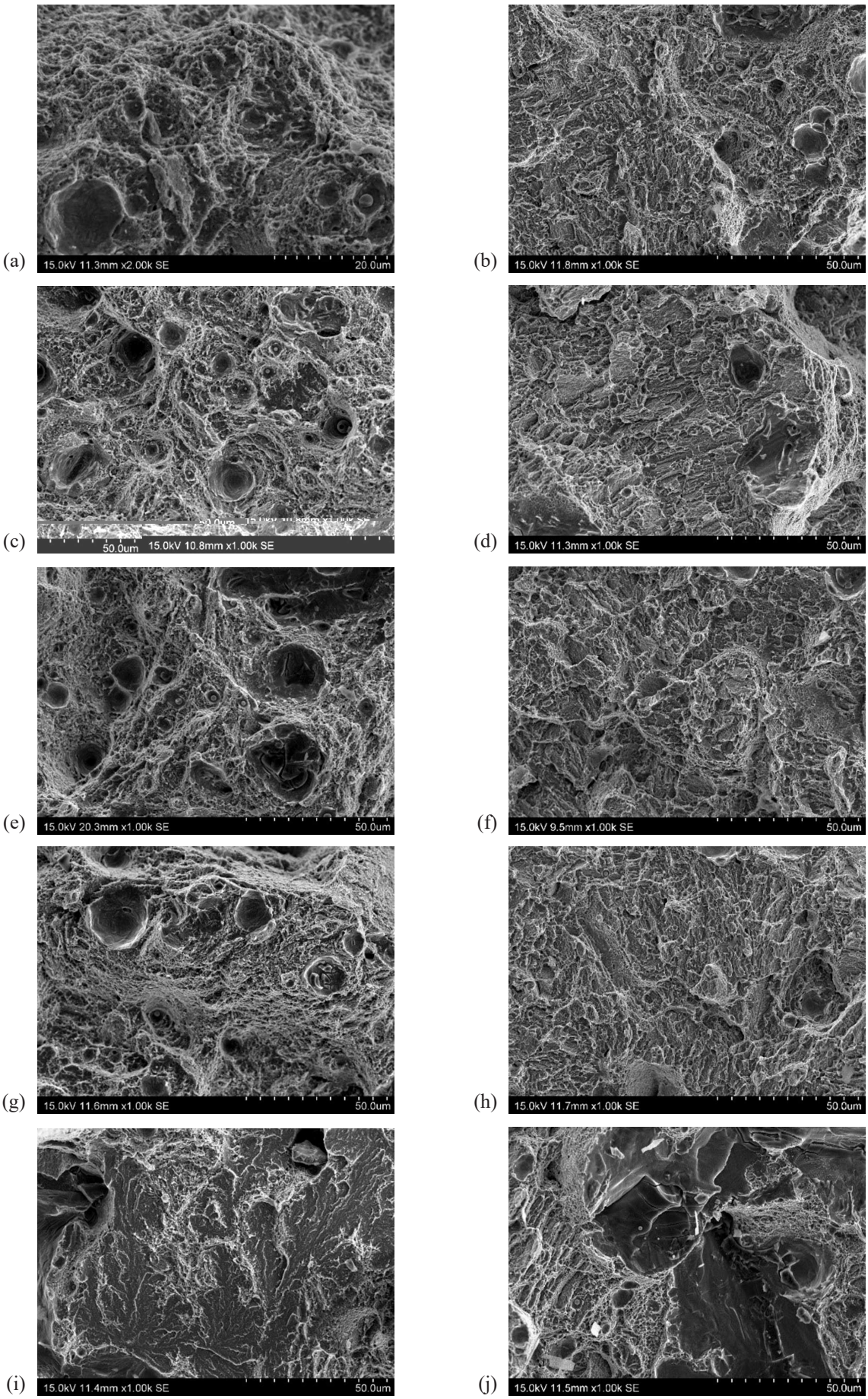

Fig. 8. Specimen fracture for different levels of triaxiality factor T_f: (a,b) 0.51; (c,d) 0.64; (e,f) 0.73; (g,h) 0.94; (i,j) 1.58 (first column of table – heat treatment "585"; second column of table – heat treatment "490")

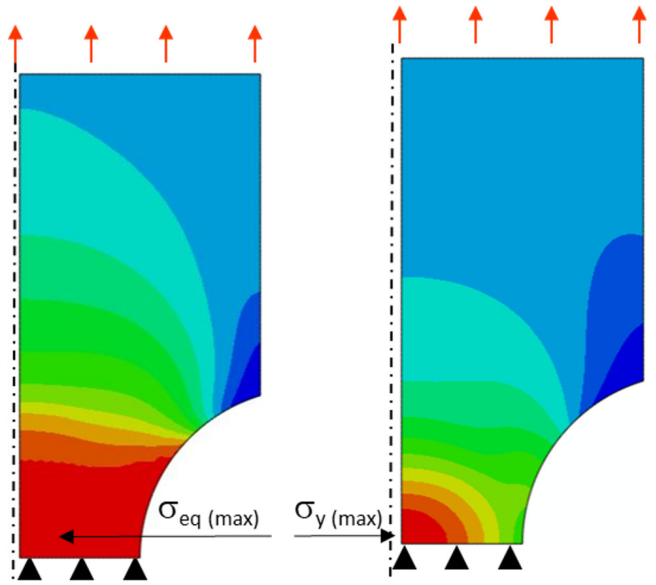

Fig. 9. Locations of areas of maximum stress σ_{max} (red) in cross-section of specimen with ring notch with radius of 3.5 mm – load at moment of failure F = 33.1 kN: (a) von Mises equivalent stress – σ_{eq}, (b) axial stress – σ_y (heat treatment variant – "585")

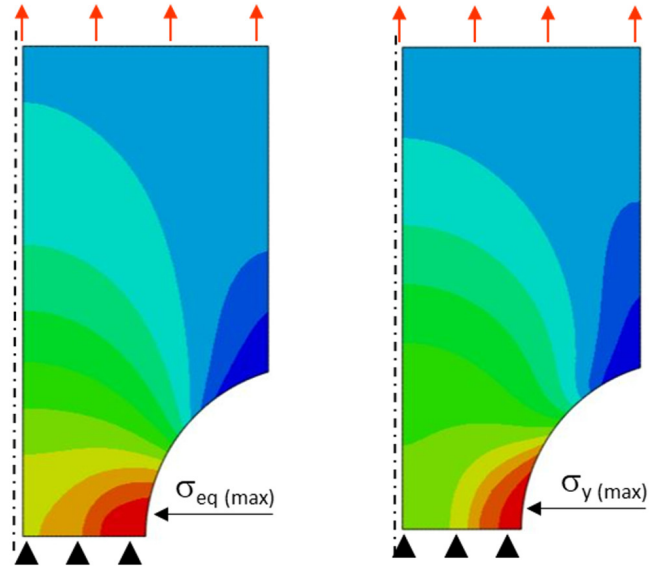

Fig. 10. Locations of areas of maximum stress σ_{max} (red) in cross-section of specimen with ring notch with radius of 3.5 mm – load at moment of failure F = 33.1 kN: (a) von Mises equivalent stress – σ_{eq}; (b) axial stress – σ_y (heat treatment variant "490")

that are typical for brittle fracture, then, the maximum value of the equivalent stress σ_{eq} and axial stress σ_y are located at the bottom of the ring notch at the moment that precedes the scrap of the sample (Figs. 10a and 10b). Based on the FEM calculations, the displacement of the element nodes at the bottom of each notch was determined and compared with the necking of the samples that were measured experimentally. Figs 11-14 show the changes of the effective strain ε_{eff} as a function of the triaxiality factor T_f for the sample that was not heat-treated (Fig. 11) and those samples after heat treatment according to variant "585" (Fig. 12), variant "540" (Fig. 13), and variant "490" (Fig. 14).

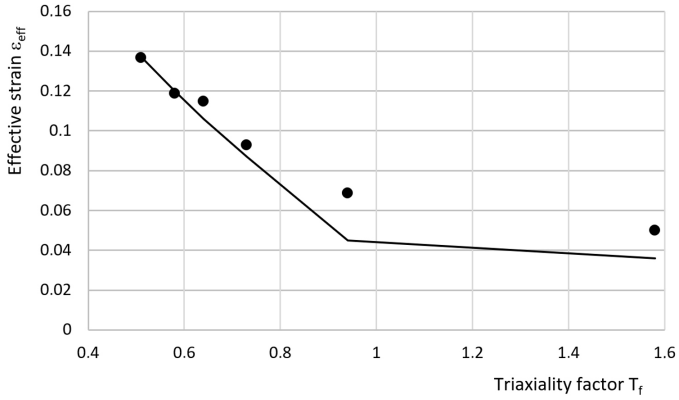

Fig. 11. Effective strain ε_{eff} at fracture as function of triaxiality factor T_f – material not heat-treated: dots – experimental measurement; solid line – FEM calculations

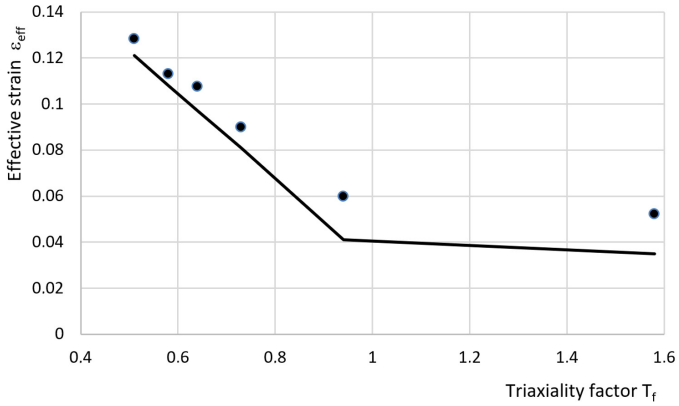

Fig. 12. Effective strain ε_{eff} at fracture as function of triaxiality factor T_f – heat-treatment variant "585": dots – experimental measurement; solid line – FEM calculations

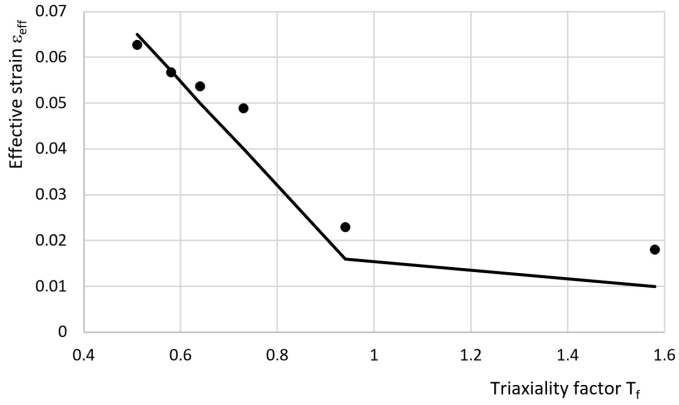

Fig. 13. Effective strain ε_{eff} at fracture as function of triaxiality factor T_f – heat-treatment variant "540": dots – experimental measurement; solid line – FEM calculations

The performed measurements and FEM calculations showed a relationship between the value of the triaxiality factor T_f and the value of the effective strain ε_{eff} of the SLM steel (visible in Figs. 10-13). The increase in the triaxiality factor that was caused by the reduction of the notch radius causes a decrease in the value of the effective strain. The process of ageing SLM steel

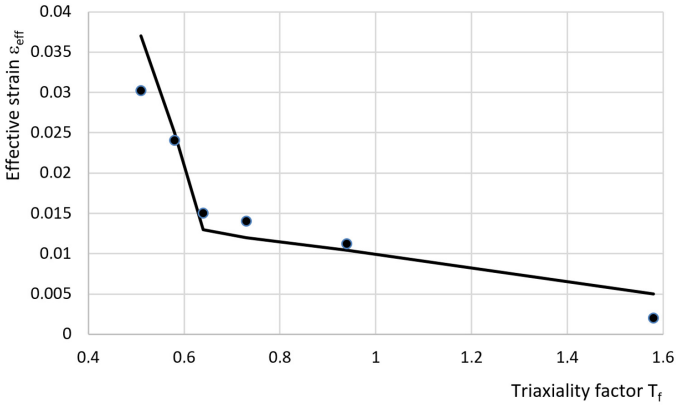

Fig. 14. Effective strain ε_{eff} at fracture as function of triaxiality factor T_f – heat-treatment variant "490": dots – experimental measurement; solid line – FEM calculations

at a temperature of 585°C causes an almost four-fold increase in the effective strain value as compared to the effective strain value that was obtained in the ageing process at 490°C for the lower values of the triaxiality factor and a seven-fold increase when the value of the triaxiality factor is about $T_f = 1.5$.

4. Discussion

Like those that are made with other methods, parts made with the use of additive technologies from steel powders are subjected to heat treatment in order to give them appropriate mechanical properties. The heat-treatment process is also carried out in the case of parts made of X3NiCoTi18-9-5 steel and obtained by the SLM method. The heat treatment of this steel is based on ageing – during which, the phases that strengthen the structure are separated. Usually, the steel-hardening process is not carried out earlier, leaving the structure as it was during the SLM process. The conducted tests were aimed at determining the influence of the selected variants of heat treatment on the strength properties of X3NiCoTi18-9-5 steel that was obtained as a result of the SLM process. In order to trace the changes in the strength, microstructure, and type of decohesion of SLM steel, a fairly wide range of ageing temperatures (from 490° to 585°C) were selected. As a result of the research, it was found that the ageing process largely influences the change of the original structure of steel that is obtained by the SLM method (as well as its mechanical properties). Increases in the ageing temperature cause decreases in the value of the ultimate tensile strength UTS, yield strength $R_{p0.2}$, and elastic modulus E, while the elongation A of the steel (measured at the moment of sample breakage) increases. As a result of heat treatment at 490°C, the steel with the highest tensile strength UTS = 1988 MPa, yield strength $R_{p0.2}$ = 1936 MPa, and modulus of elasticity E = 183,300 MPa was obtained when compared to the material that was tested immediately after printing (for which, the above values were UTS = 1084 MPa, $R_{p0.2}$ = 1936 MPa, and E = 162,300 MPa, respectively. Ageing at a temperature of 490°C resulted in the greatest reduction in the value of the elongation during the sample's fracture as compared to the elongation of the untreated material. The elongation value of the tested samples after ageing at 490°C was A = 5.4% on average, while the samples that were not subjected to ageing showed an average elongation of A = 18.2%. The results of the measurements of the elongation of the samples using the extensometer also had a much larger dispersion of values as compared to the other measured values, such as the yield strength, ultimate tensile strength, and elastic modulus. The reason for this may have been the occurrence of small internal defects that significantly reduced the plasticity of the material. The increase in strength and decrease in elongation that occurred as the ageing temperature increased were caused by the increasing reversion of austenite, which is released at the grain boundaries at 540°C and inside the cells at 585°C also inside the cells Fig. 6. The results of the static tensile test for aged and non-heat treated specimens are summarized in TABLE 3.

TABLE 3

Results of uniaxial tensile test

Variant of heat treatment	$\sigma_{p0.2}$ (MPa)	UTS (MPa)	E (MPa)	A (%)
Not heat-treated	1084 (7)	1170 (10)	162,300 (300)	18.2 (0.2)
"490"	1936 (18)	1988 (7)	183,300 (400)	5.4 (2.7)
"540"	1696 (21)	1743 (23)	179,800 (8300)	6.3 (3.1)
"585"	1415 (8)	1486 (16)	175,300 (3200)	15.1 (1.3)

In order to determine the influence of the triaxiality factor T_f on the decohesion process of SLM steel for the material not heat-treated and after aging at the temperature of 490, 540 and 585°C a static tensile test was performed for ring-noched samples with different radii. The size of the notch radius affects the value of triaxiality factor determined by the Bridgman Eq. (1). An increase in the value of the triaxiality factor T_f determined on the basis of Eq. (2) causes an increase in the maximum force recorded during the static tensile test (Fig. 4), regardless of the variant of the heat treatment performed. The aging temperature also influences the values of the maximum force recorded during the tensile test of samples with a ring notch. The highest value of the force during the tests was recorded when the aging temperature of the samples was 490°C. On the other hand, an increase in the triaxiality factor causes a decrease in the value of the effective strain ε_{eff} measured in the plane of the notch, calculated using the FEM method and Eq. (3). The value of the effective strain also depends on the variant of the performed heat treatment. Aging at 585°C causes the greatest deformation.

Fractographic examinations of fractures of the notched samples with the use of a scanning microscope and numerical calculations confirmed the influence of the size of the notch radius and the aging temperature on the decohesion of X3NiCoTi18-9-5 steel obtained by the SLM method. According to

the literature data, the conducted research confirmed that the increase in the triaxiality factor for each heat treatment variant causes a greater probability of a brittle fracture of the material.

It was found that for each variant of the applied heat treatment, it is possible to indicate an approximate limit value of the triaxiality factor, above which the brittle SLM steel scrap occurs. This value is determined by the characteristic bend of the line of the relationship between the triaxiality factor and the effective strain determined on the basis of numerical calculations, visible in Figs. 11-14 by a continuous line. A similar course of this relationship, also shown in Figs. 11-14, was found on the basis of experimentally measured changes in the diameter in the bottom of the notch before and after the tensile test and determination of the effective strain ε_{eff} on the basis of Eq. (3). As a result of the fractography tests, it was found that after aging at 585 and 540°C the fracture surface of the samples shows a dominant share of the plastic fracture below the value of the triaxiality factor of T_f = 0.9. In the photos of the fractures of the samples aged at 585°C, shown in Figures 8a,c,e,g,i), the share of the brittle scrap is only visible in Figs. 8i and 8g. In the case of the samples that were aged at a temperature of 490°C, the value of the triaxiality factor that was determined on the basis of the course of the function $\varepsilon_{eff} = f(T_f)$ was approximately 0.6. The scanning photos of the breakthroughs of the samples aged at 490°C that are shown in Figs. 8d,f,h, and i reveal the brittle fracture characteristics. If the triaxiality factor does not exceed the values given above (T_f = 0.6 and T_f = 0.9 for the analysed "490" and "585" ageing variants, respectively), then the maximum value of the axial stress σ_y at the moment of scrapping each sample occurs at the point of the intersection of its axis with the symmetry plane of the ring notch according to the numerical calculations. In the above case, the numerically determined values of the stresses and the position of the maximum axial stresses σ_y are consistent with Bridgman's analytical solution. On the other hand, if the triaxiality factor is greater than T_f = 0.9 for samples that are aged at 540° and 585°C and greater than T_f = 0.6 for samples that are aged at 490°C, then the maximum value of axial stress σ_y and the value of equivalent stress σ_{eq} at the moment that a specimen cracks occur not in the specimen's axis but at the bottom of the notch according to the von Mises hypothesis (Fig. 10).

5. Conclusion

As a result of our research, it was found that the types of fractures of samples that are obtained from X3NiCoTi18-9-5 steel powder by the SLM method depends on the size of the ring notch radius. This is because the size of the notch radius affects the stress state in the notch plane. The location of the area of maximum axial stress σ_y and equivalent stress σ_q at the time of sample decohesion depends on the size of the radius ρ. The state of the stress can be characterised by the value of the so-called triaxiality factor that is calculated theoretically on the basis of Bridgman's solution or numerically. In addition to the triaxiality factor being directly related to the size of the notch radius and the sample diameter in the plane of the notch bottom as determined by Eq. (2), the type of the SLM steel decohesion also depends on the ageing temperature. Based on the performed numerical calculations and experimental tests, it was found that, for each of the analysed variants of heat treatment, it was possible to indicate the approximate limit value of the triaxiality factor T_f, above which there is a scrap of brittle X3NiCoTi18-9-5 steel produced by the SLM method. This value is determined by the characteristic bending of the function that determines the relationship between the triaxiality factor T_f and effective strain ε_{eff}.

Funding

This research was supported by the National Centre for Research and Development in the framework of "Ścieżka dla Mazowsza". This program is under the project "Development and commissioning of an innovative die-casting technology with the use of targeted crystallization used to improve the quality of the structure and surface of small-sized details" No. MAZOWSZE/0011/19.

Acknowledgments

Thanks to the RCiT company from Radom, Poland, for their cooperation and for enabling the production of samples that were necessary for the implementation of our research.

REFERENCES

[1] D. Herzog, V. Seyda, E. Wycisk, C. Emmelmann, Acta Materialia **117**, 371-392 (2016). DOI: https://doi.org/10.1016/j.actamat.2016.07.019

[2] C.Y. Yap, C.K. Chua, Z.L. Dong, Z.H. Liu, D.Q. Zhang, L.E. Loh, S.L. Sing, Applied Physics Reviews **2**, 041101 (2015). DOI: https://doi.org/10.1063/1.4935926

[3] E.O. Olakanmi, R.F. Cochrane, K.W. Dalgarno, Progress in Materials Science **74**, 401-477 (2015). DOI: https://doi.org/10.1016/j.pmatsci.2015.03.002

[4] J. Piekło, A. Garbacz-Klempka, Archives of Foundry Engineering **21** (2), 9-16 (2021). DOI: https://doi.org/10.24425/afe.2021.136092

[5] I. Yadroitsev, P. Krakhmalev, I. Yadroitsava, S. Johansson, I. Smurov, Journal of Materials Processing Technology **213** (4), 606-613 (2013). DOI: https://doi.org/10.1016/j.jmatprotec.2012.11.014

[6] Y. Kajimaa, A. Takaichia, T. Nakamotob, T. Kimurab, N. Kittikundechaa, Y. Tsutsumic, N. Nomurad, A. Kawasaki, H. Takahashie, T. Hanawac, N. Wakabayashi, Journal of the Mechanical Behavior of Biomedical Materials **78**, 1-9, (2018). DOI: https://doi.org/10.1016/j.jmbbm.2017.11.009

[7] R. Branco, J.D. Costa, J.A. Martins Ferreira, C. Capela, F.V. Antunes, W. Macek, Materials and Design **201** (2021). DOI: https://doi.org/10.1016/j.matdes.2021.109469

[8] M.C. Brennan, J.S. Keist, T.A. Palmer, Journal of Materials Engineering and Performance **30**, 4808-4818 (2021). DOI: https://doi.org/10.1007/s11665-021-05919-6

[9] W. Wu, X. Wang, Rapid Prototyping Journal, (2020). DOI: https://doi.org/10.1108/RPJ-08-2018-0189

[10] I. Milne, R.O. Ritche, B.L. Karihaloo, Comprehensive structural integrity, Amsterdam: Elsevier, Pergamon (2003).

[11] J. Lachowski, J. Borowiecka-Jamrozek, Archives of Foundry Engineering **21** (2), 29-34 (2021). DOI: https://doi.org/10.24425/afe.2021.136094

[12] J. Piekło, M. Małysza, R. Dańko, Archives of Civil and Mechanical Engineering **18**, 1300-1308 (2018). DOI: https://doi.org/10.1016/j.acme.2018.03.007

[13] J. Piekło, M. Maj, Archives of Foundry Engineering **9** (2), 25-28 (2009).

[14] P.W. Bridgman, Studies in Large Flow and Fracture, Mc Graw-Hill, New York (1952).

[15] F. Rivalta, L. Ceschini, A.E.W. Jarfors Roland, R. Stolt, Metals **11**, 1-31 (2021). DOI: https://doi.org/10.3390/met11050826

[16] J. Piekło, Zastosowanie metody przyrostowej SLM do wykonania wybranych elementów układu chłodzenia form ciśnieniowych, Wydawnictwo Naukowe Akapit, Kraków (2019).

[17] J. Piekło, A. Garbacz-Klempka, Materials **13** (23), 5533 (2020). DOI: https://doi.org/10.3390/ma13235533

[18] R. Casati, J.N. Lemke, A. Tuissi, M. Vedani, Metals **6**, 218 (2016). DOI: https://doi.org/10.3390/met6090218

[19] F.F. Conde, J.D. Escobar, J. Rodriguez, C.R.M. Afonso, M.F. Oliveira, J.A. Avila, Journal of Materials Engineering and Performance **30**, 4925-4936 (2021). DOI: https://doi.org/10.1007/s11665-021-05553-2

[20] W.K. Law, KC Wong, H. Wang, Z. Sun, C.L. Lim, Journal of Materials Engineering and Performance **30**, 6389-6405 (2021). DOI: https://doi.org/10.1007/s11665-021-05948-1

[21] E. Yasa, K. Kempen, J.P. Kruth, Microstructure and mechanical properties of maraging steel 300 after selective laser melting. In: Proceedings of the Solid Freeform Fabrication Symposium Proceedings, Austin, TX, USA (2010).

[22] Y. Bai, D. Wang, Y. Yang, H. Wang, Material Science and Engineering. A, **760**, 105-117 (2019). DOI: https://doi.org/10.1016/j.msea.2019.05.115

[23] K. Kempen, E. Yasa, L. Thijs, J.P. Kruth, J. Van Humbeeck, Phys. Procedia **12**, 255-263 (2011).

[24] J. Piekło, A. Garbacz-Klempka, Effect of heat treatment of the microstructure and mechanical properties of the maraging steel produced by Selective Laser Melting process intended to make parts of a die casting die, in: J.J. Sobczak, P. Zięba, (Eds.), Metalurgia 2020, Gliwice (2021).

[25] SIMULIA Dassault System, Abaqus analysis user's manual, 2019.

[26] M. Biel-Gołaska, Fatigue & Fracture of Engineering Materials & Structures **21**, 965-975 (1998).